Distinct sensorimotor feedback loops for dynamic and static control of primate precision grip

Tomomichi Oya[1,2†], **Tomohiko Takei**[1,2†‡], **Kazuhiko Seki**[1,2*]

***For correspondence:** seki@ncnp.go.jp (K.S.)

[†]These authors contributed equally to this work

Present address: [‡]Department of Physiology and Neurobiology, Graduate School of Medicine/ The Hakubi Center for Advanced Research, Kyoto University, Kyoto, Japan

[1]Department of Neurophysiology, National Institute of Neuroscience, National Center of Neurology and Psychiatry, Tokyo, Japan; [2]Department of Developmental Physiology, National Institute for Physiological Science, Aichi, Japan

Abstract Volitional limb motor control involves dynamic and static muscle actions. It remains elusive how such distinct actions are controlled in the central nervous system through separated or shared neural circuits. Here we explored the potential separation of neural circuitry for dynamic and static controls in the primate hand actions. We investigated the neuronal interactions between the spinal cord and forelimb muscles, and the motor cortex and the muscles, with an emphasis on their modulation during dynamic and static phase of grasping. While macaque monkeys were performing a precision grip comprising dynamic and static phases, we recorded spinal or cortical local field potentials simultaneously with electromyographic activity, thereafter examined neural coherence between the signals. We observed the emergence of beta-range neural coherence with muscle activity at spinal cord and motor cortex in the separated phases; spinal coherence during the grip phase and cortical coherence during the hold phase. Further, both of the coherence were influenced by bidirectional interactions with reasonable latencies as beta oscillatory cycles. These results indicate that dedicated feedback circuits comprising spinal and cortical structures underlie dynamic and static control of dexterous hand actions.

Introduction

Our motor behaviors comprise a continuum of "moving" a limb and "holding" it still, through dynamic and static control of muscle activity. The control of such distinctive modes appears contrasting. During a dynamic movement, the trajectory and speed are often required to be controlled, whereas holding-still requires the stability of the muscle force. To meet such distinct requirements, it may be beneficial for the neural system to accommodate separate circuits for each control. Indeed, the mammalian central nervous system (CNS) houses such dedicated circuits in the brainstem for the dynamic and static control of saccadic eye movement (***Robinson, 1973***). This separation has been proposed as a potentially common design principle among motor end-effectors (***Shadmehr, 2017***).

However, for the skeletomotor control, it is largely unknown whether such distinct circuits are at work, except that some literature support the concept. A subgroup of neurons situated in the rostral part of the motor cortex predominantly exhibited phasic discharges during the dynamic phase (***Crammond and Kalaska, 1996***; ***Shalit et al., 2012***). In contrast, a greater population of tonic discharges during the static phase was reported in the caudal part of the motor cortex (***Crammond and Kalaska, 1996***; ***Shalit et al., 2012***), and the premotoneuronal cells with direct connections to the spinal motoneurons, such as corticomotoneuronal (CM) cells (***Maier et al., 1993***) and premotor spinal interneurons (***Takei and Seki, 2013a***). While these studies suggest cortical and spinal neurons

are involved in dynamic and static control, a deficiency in these results is the unresolved effective connectivity of the population neuronal activity to the muscular outputs; albeit the individual premotoneuronal cells could affect the target motoneuron activities, their spatial or temporal properties are often incongruent with the target muscles (***Takei and Seki, 2013b***; ***Griffin et al., 2015***).

Therefore, it is crucial to directly examine an effective connectivity of the population neural activity with muscular outputs, such as coherence analyses between local field potentials (LFPs) of neural structures and electromyography (EMG) (***Baker, 2007***; ***Pesaran et al., 2018***). Although a coherent oscillation has been demonstrated between an LFP of the motor cortex and EMG at a beta frequency range (15–30 Hz) during a sustained control of muscle action (***Conway et al., 1995***; ***Baker et al., 1997***; ***Salenius et al., 1997***; ***Kilner et al., 1999***; ***Gross et al., 2000***; ***Divekar and John, 2013***), it is uncertain for the separation of neural circuitry underlying dynamic and static skeletomotor control, since 1) comparable beta-range coherent oscillations with muscles have not been found during the dynamic phase, and 2) it remains unresolved how such coherent oscillations are generated, namely, whether they arise from an efferent entrainment of oscillatory cortical drive transferred to the muscles (***Gerloff et al., 2006***), or from a reciprocal interaction of motor commands and sensory feedbacks between the motor cortex and the muscles (***Baker, 2007***; ***Aumann and Prut, 2015***). To address these issues, we sought a potential coherent oscillation with muscles in the spinal cord as well as in the motor cortex, since spinal interneurons receive convergent inputs from the descending pathways including the corticospinal and other tracts (***Riddle and Baker, 2010***), and spinal premotor interneurons are clearly discharged in relation to the dynamic and static muscle activity (***Takei and Seki, 2013a***). Also, we sought to disambiguate the two possible mechanisms for emergence of neural coherence in a more decisive way by delineating information flows and the time lag estimates between coherent signals.

We analyzed neural coherence and information flows between LFPs from the spinal cord and the motor cortex, and EMG activity of the forearm, while the macaque monkey performed a precision grip task that involved both dynamic grip and static hold controls. We found the emergence of significant spinomuscular and corticomuscular coherence as distinct time-frequency patterns relevant to the dynamic and static grip phases. Furthermore, directional information analyses indicate that spinal and cortical beta-range coherence are composed of a reciprocal interaction with the muscles, with corresponding time lags for beta oscillations. We also show that these two feedback loops differ in the muscles involved (i.e., spinal local feedback vs. cortical divergent feedback loops). These results indicate that distinct sensorimotor feedback loops are engaged in the dynamic and static control of precision grip of primates.

Results

Experiment, behavior, and analyses

We recorded LFP signals from four macaque monkeys using single microelectrodes in conjunction with EMG activity from the forelimb muscles (Figure 1A, C; see Table S1 for muscle lists for each monkey) while each monkey was performing a precision grip task involving dynamic grip (grip) and static hold (hold) periods. The monkeys were instructed to acquire visual targets that represented lever positions, by pinching a pairs of spring-loaded levers with the thumb and index finger (Figure 1B). Spinal LFP signals were recorded from four monkeys, and the analyzed signals included 4 LFPs and 2 EMGs from monkey U, 7 LFPs and 19 EMGs from monkey A, 72 LFPs and 20 EMGs from monkey E, and 1 LFP and 21 EMGs from monkey S; cortical LFP signals were obtained from two monkeys: 71 LFPs and 20 EMGs from monkey E, and 26 LFPs and 21 EMGs from monkey S. LFP-EMG pairs with electrical cross talk were excluded from the analysis (see Materials and Method). The summaries for analyzed LFP–EMG pairs are summarized in Table S2.

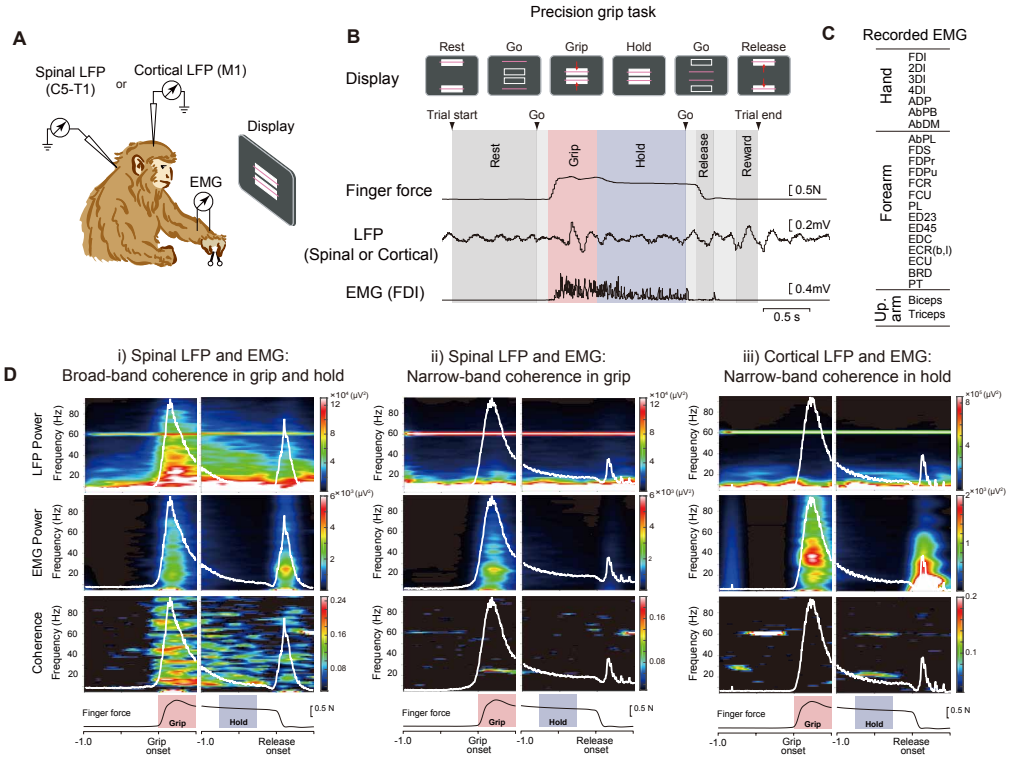

Figure 1. A. Task and recording setup. Monkeys performed a precision grip task by squeezing a pair of spring-loaded pivoted levers; they were instructed to align the bars (corresponding to lever displacements) to prescribed rectangle areas in the front display. During the task either spinal or cortical local field potentials (LFPs) were recorded in conjunction with electromyography (EMG) of forelimb muscles. **B.** Task epochs delineated by events, and exemplar raw traces of finger force (sum of two lever forces), LFP, and EMG. On the visual and auditory cue, the monkey squeezes the levers (grip phase: red-shaded area) maintains the force for 1–2 s (hold phase: blue-shaded area). **C.** A list of forelimb muscles recorded in the present study (for each animal, see Table S1). **D.** Representative patterns of coherence (bottom) and the underlying power spectra (top) of spinal broad-band (i)), spinal narrow-band (ii)) or cortical narrow-band (iii)) LFPs and the corresponding EMGs (middle: AbPB for i), AbPL for ii), and AbDM for iii)). White traces indicate these EMG patterns.

Distinct types of time-frequency coherence patterns: spinal broad-band, spinal beta-band, and cortical beta-band coherence

To examine the overall time-frequency patterns in coherence, we applied wavelet transformation on LFP and EMG signals with respect to grip onset or release onset (from 1 s before and 0.5 s after the onsets), both of which were then processed for spectral analysis (Figure 1D). We found three major types of coherence patterns in the spinomuscular or corticomuscular coherence. Spinomuscular coherence exhibited two types: one was termed spinal broad-band coherence, which exhibited paralleled temporal evolution with that of the paired EMG pattern, namely phasic-tonic activity during grip—hold phases (Figure 1D-i); the other was termed spinal narrow-band coherence in the beta range, which markedly emerged during the grip phase (Figure 1D-ii). In contrast, corticomuscular coherence appeared as a narrow band in the beta-range, being pronounced specifically during the hold phase (Figure 1D-iii).

To objectively classify these time-frequency patterns, we measured the following two features of coherence: 1) the integral of the contours in the wavelet coherence (Figure S1A-i), 2) the frequency width of coherence in a fixed-time period as a supplement (Figure S1A-ii, see Materials and Methods for the detail). The integral of the contours in the wavelet coherence during the grip (0–1 s from the grip onset) or hold phase (-1–0 from the release onset) was calculated as the sum of significant areas at each contour level. With this measurement, we found a bimodal distribution for spinomuscular

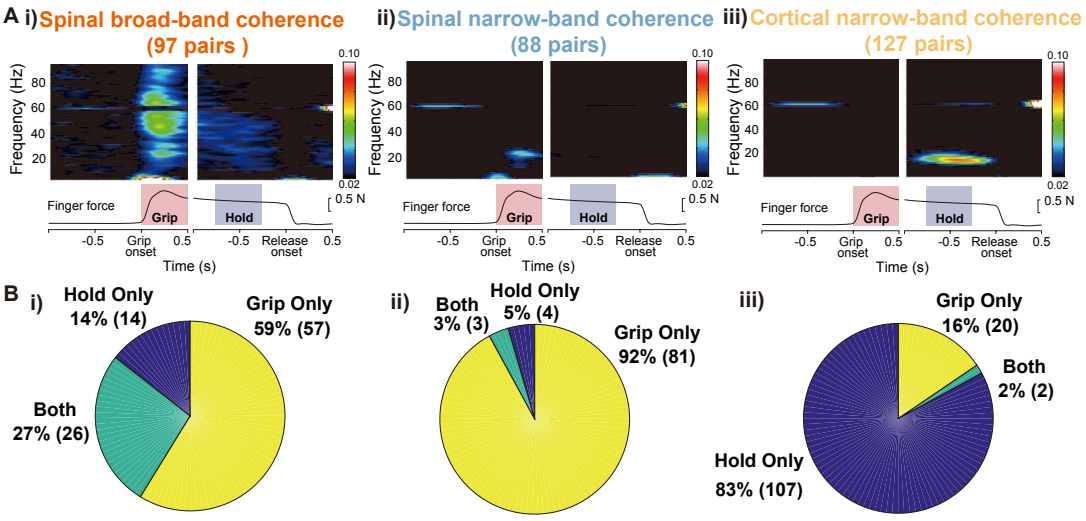

Figure 2. Group averages and proportions in significant pairs in grip vs. hold phases of each coherence pattern. **A.** Averaged wavelet coherence patterns classified according to the distributions shown in Fig S1B. **B.** The proportions of significant pairs in grip, hold, and both phases for each classified coherence pattern. i) Spinal broad-band pattern (BB) spans wide frequency and time ranges over the grip and hold phases (83 out of 97 pairs for grip, 40 out of 97 pairs for hold). ii) Spinal narrow-band (NB) pattern emerges in the beta band ruing the grip phase (84 out of 88 pairs). iii) Cortical narrow-band (NB) pattern is pronounced in the beta range during the hold phase (107 out of 127 pairs).

coherence (Figure S1B-i), which was successfully separated using a Gaussian mixture model (GMM). The two separated distributions were assigned to the narrow-band type (blue, Figure S1B-i), and the broad-band type (red, Figure S1B-i), respectively. This dissociation was largely consistent with the distributions in frequency width (Figure S1B-i, vertical histogram) as was used in a previous study (***Takei and Seki, 2008***). For corticomuscular coherence we saw solely unimodal distributions in both frequency width and contour integrals (Figure S1B-ii), which led us to define all of them as narrow-band.

Classified spinomuscular broad-band coherence (97 pairs in total) manifested itself not only in the grip phase but also in the hold phase (Figure 2A-i), with c.a. 90% of pairs and c.a. 40% of pairs showing significant coherence during the grip and hold phases, respectively (Figure 2B-i). Spinal narrow-band coherence (88 pairs in total) emerged in the beta band, predominantly during the grip phase (Figure 2A-ii) with more than 90% pairs showing significance exclusively during the grip phase (Figure 2B-ii). This was in a clear contrast with cortical narrow-band coherence (127 pairs in total), which was evident almost exclusively during the hold phase (Figure 2A-iii), with more than 80% pairs being significant only during the hold phase (Figure 2B-iii).

To further explore the functional differences among the coherence types, we examined which individual muscles were coherent with the spinal or cortical LFPs (Figure 3). Overall, the coherent LFP—muscle pairs were observed predominantly in intrinsic hand, extrinsic hand, and wrist flexor muscles. Spinal broad-band patterns (red-shaded area in Figure 3A) were most widely distributed among those observed muscles, showing reflection of all recruited muscles. Spinal narrow-band coherence (blue shaded areas in Figure 3A and B) showed a preference in the index finger muscles, i.e., FDI and FDPr. This specific preference was contrasted with a relatively wider distribution of the cortical narrow-band coherence observed in the finger muscles (yellow shaded area in Figure 3B).

While a substantial proportion of significant pairs in both types of spinal coherence patterns were found in the grip phase, a significant difference in latency was observed with respect to grip onset (Figure S2). Spinal broad-band coherence was distributed with the median value of 95 ms prior to grip onset, whereas spinal beta-band was distributed with the median value of 7 ms prior to grip onset (*t*-test with unequal variance, $p < 0.001$). The latency of the spinal broad-band coherence

indicates that the onset occurred prior to grip onset, as well as spinal beta-band coherence onset by c.a. 100 ms.

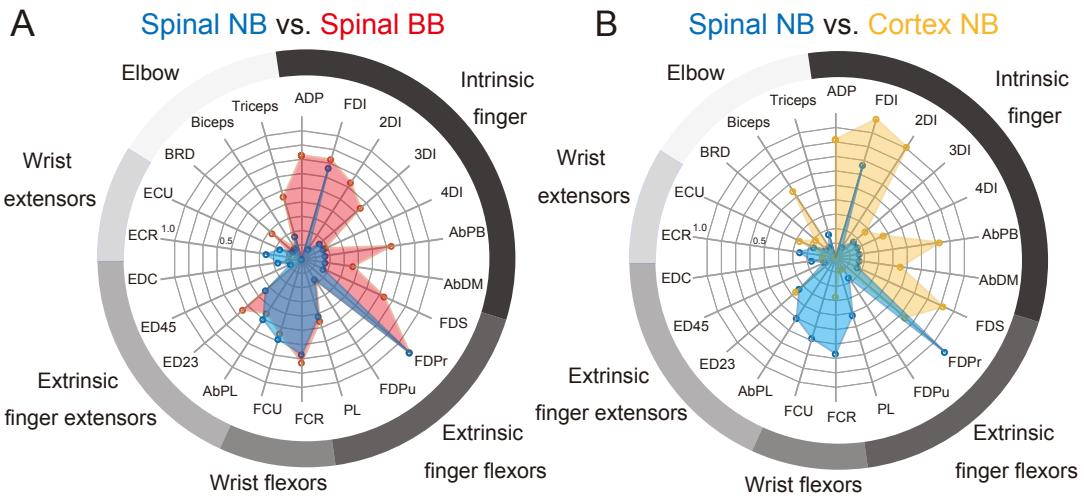

Figure 3. Muscle distributions of LFP–EMG coherent pairs for spinal NB (blue), spinal BB (red) and cortical NB (yellow) groups. Muscles are ordered clockwise from intrinsic finger muscles, extrinsic finger flexors, wrist flexors, extrinsic finger extensors, wrist extensors, to elbow muscles. **A.** Comparison of the distributions between spinal NB (blue) and spinal BB (red) coherent pairs. The muscles are generally overlapped except the spinal NB pairs, which are predominantly partial to FDI and FDPr, both acting in index finger flexion. This is in contrast to a broader distribution of spinal BB pairs, reflecting recruitment of intrinsic finger, extrinsic finger, and wrist flexor muscles in the precision grip. **B.** Comparison of the distributions between spinal NB (blue) and cortical NB (yellow) coherent pairs. A preference of spinal NB to the index finger muscles (FDI and FDPr) is clearly contrasted with cortical NB, which shows rather even distribution to the finger muscles recruited.

Differences in frequency, phase and inter-muscle connections between spinal and cortical coherence in the beta range

We then sought to determine whether there exists a difference between the spinal and cortical narrow-band patterns, by comparing frequency and phase distributions between the two coherence patterns (Figure 4). We observed a difference in the normalized frequency distribution between them, where spinal narrow-band coherence showed a slightly higher frequency content than that for cortical narrow-band (Figure 4A). We also found each phase distribution clustered to a specific angle (Rayleigh test, $p < 0.001$ for each) where the spinal narrow-band lagged behind the muscle activity (Figure 4B-i), whereas the cortical narrow-band occurred prior to the muscle activity (Figure 4B-ii). These two distributions were statistically different (Mardia–Watson–Wheeler test, $p < 0.001$). These results indicate that the spinal and cortical narrow-band coherence patterns may have arisen from different interaction processes, albeit in close frequency bands.

Furthermore, we frequently observed coherence between an LFP and multiple EMGs at a given recording site, which may imply an interaction between the muscles through a shared network. As such, we defined the muscles that simultaneously emerged at a given site as interacting muscles mediated by spinal or cortical narrow-band coherence, and counted the number of combinations of those muscles for each spinomuscular and corticomuscular coherence. Consequently, a marked contrast was found in the inter-muscle connections between the spinal and cortical narrow-band coherence; for spinomuscular coherence (104 pairs in 21 sites) the interacting muscles were predominantly clustered in the forearm flexors (extrinsic hand and wrist flexors) (Figure 5A). In contrast, for corticomuscular coherence (59 combinations in 28 sites) there were divergent connections among the muscles, ranging from the intrinsic hand muscles to upper arm muscles (Figure 5B).

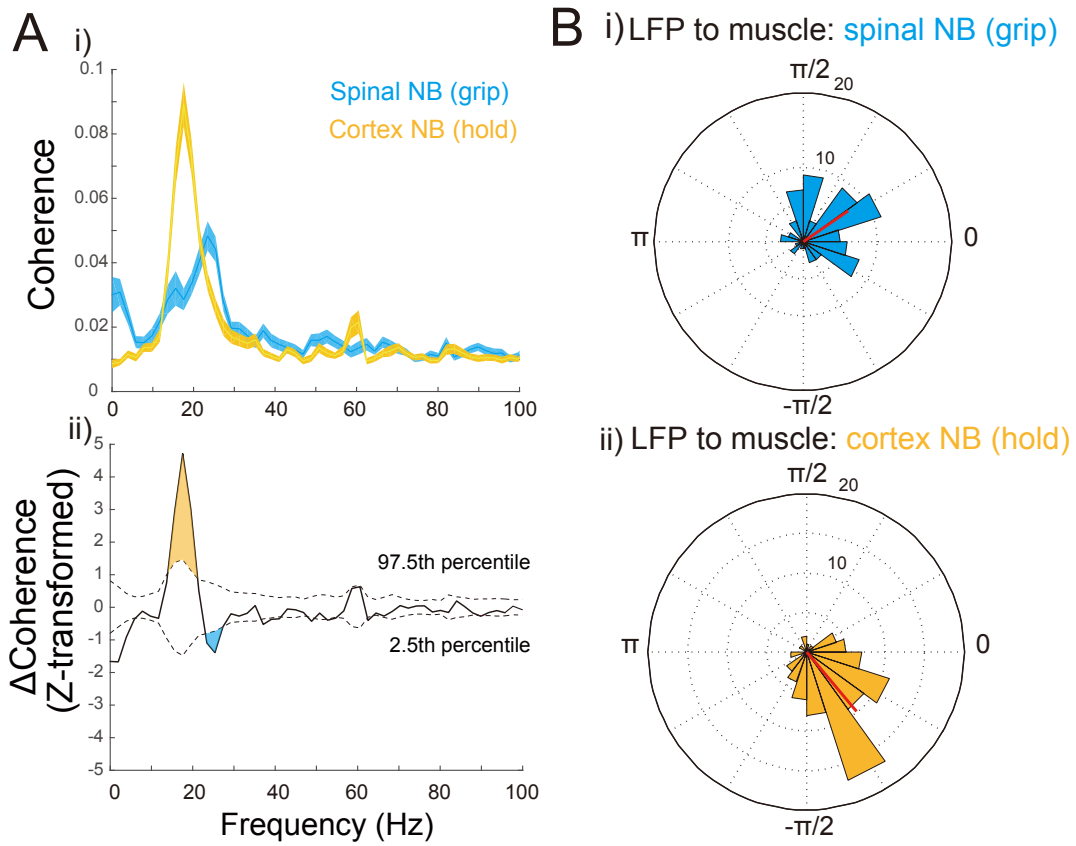

Figure 4. Comparison of frequency **(A)**, phase **(B)** distributions between the spinal narrow-band coherence during the grip phase (spinal NB) and the cortical narrow-band coherence during the hold phase (cortical NB). **A.** i) Frequency distributions for the mean for spinal NB (blue, n = 88) and cortical NB (orange, n = 127). The peak frequency for the spinal NB is 23.4 Hz and that for the cortical NB is 17.5 Hz (Shaded areas are $\pm SEM$). ii) Differences between the mean coherence values (Z-transformed). Dashed lines denotes 97.5th and 2.5th confidence intervals obtained from the Monte-Carlo method (10000 iterations). The orange-shaded area represents the frequency band where cortical NB is greater than spinal NB, and blue-shaded area indicates the band where spinal NB is greater than cortical NB. **B.** i), ii) Phase distributions for the spinal NB and cortical NB show clustered angles (0.59±1.19, -0.87±0.91, mean±SD, as represented by red vectors, Rayleigh test, $p < 0.001$ for each), which are statistically inhomogeneous (Mardia-Watson-Wheeler test, $p < 0.001$).

Direction of causality in spinomuscular and corticomuscular coherence

We further examined whether the observed coherence reflects putatively causal interactions with a particular direction. To explore the direction of an influence and its phase–lag relationship between the neural structures and muscles, we used a combination of directed and partial directed coherence measures based on Granger causality and a multivariate autoregressive (MVAR) model; each measure is complementary to each other in determining a causality and estimating the lag (see Materials and Methods for details). We found that spinal broad-band coherence predominantly comprised an efferent pathway with relatively weak beta afferent components (Figure 6A-i, B-i), whereas spinal beta-band coherence in the grip phase comprised bidirectional interactions in the beta range with dominant afferent components (Figure 6A-ii). Corticomuscular coherence comprised a beta-range bidirectional interaction between the afferent and efferent pathways with dominant efferent components (Figure 6B-iii). The phase delay of spinal broad-band coherence was c.a. 8.0 (±5.6, quantile) ms for the efferent components (Figure 7A-i, B-i), consistent with the conduction delay between the spinal motoneurons and the muscles (***Maier et al., 1998***). For spinal narrow-band coherence, the beta-band afferent and efferent delays were 26.8 (±14.8) and 30.2 (±7.3) ms (Figure 7A-ii), respectively. For cortical beta-band coherence the delays were 27.0 (±8.7)

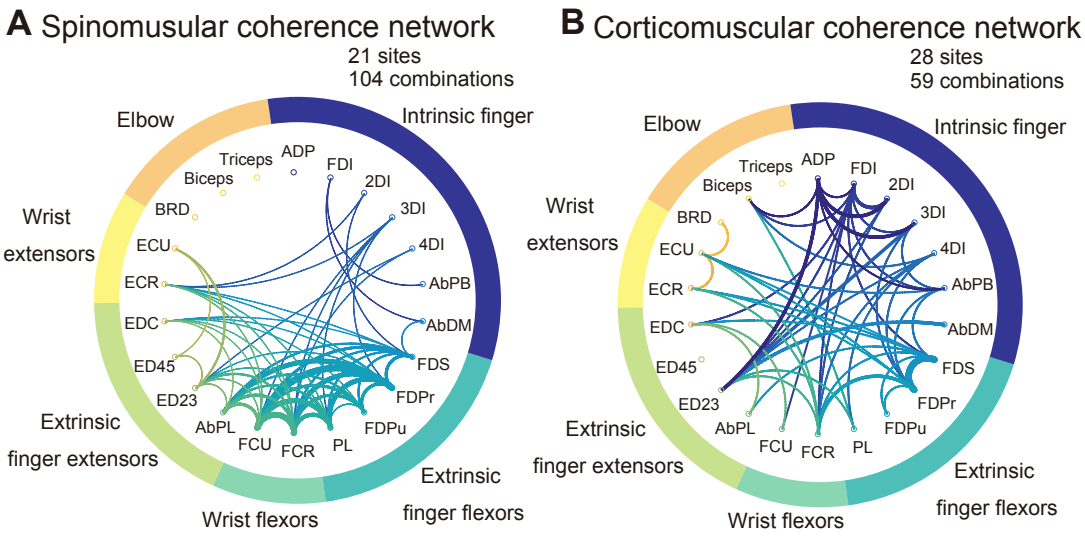

Figure 5. Comparison of putative inter-muscle connections through spinal (**A**) and cortical (**B**) narrow-band coherence. The thickness of the line represents the number of connections observed between the muscles; the thinnest line denotes the minimum connection of a value of 1 (e.g., FDI and AbPB in **A**), whereas the thickest line indicates the maximum connection as a value of 7 (e.g., FDPr and FCU in **A**). i)The connections mediated by spinomuscular NB coherence are predominantly found among synergistic muscles, i.e., extrinsic finger flexors and wrist flexors. ii) The connections mediated by the corticomuscular NB coherence are observed in diverse combinations of muscles across the forelimb, ranging from the intrinsic hand to the upper arm muscles.

and 25.7 (±14.1) ms (Figure 7, B-iii). It is notable that the aggregate median for the entire delay for spinomuscular and corticomuscular coherence (i.e. sums of afferent and efferent delays) was c.a. to 50–60 ms, a reciprocal of the central frequency of the coherence (c.a. 15–20 Hz). These results corroborate the hypothesis that the beta-band corticomusuclar coherence is the result of bidirectional interactions between the cortex and the periphery, which is, further applicable to spinomuscular coherence.

Discussion

It has been unclear whether distinct circuits are engaged in dynamic vs. static control of limb muscle actions. We found that the beta-range neural coherence with muscles emerged in the spinal cord and motor cortex, each of which was distinctively evident during dynamic or static phases of precision grip. Furthermore, neural information flows were bidirectional in both of beta-range spinomuscular and corticomuscular coherence with reasonable latencies for beta oscillatory cycles, indicating dedicated feedback loops underlie each coherent pattern. The muscle groups involved in each coherence are also distinct; the trans-spinal loop involves the prime movers of the precision grip muscles with interactions among local forearm flexors, whereas the trans-cortical feedback loop arise largely through the recruited finger muscles, with divergent interactions across the forelimb joints.

Spinal broad-band coherence reflects population motoneuron pool activity

In our previous study, we reported broad-band coherence between the spinal LFP and a forelimb muscle. Further, in light of the wide frequency-range correlation (i.e., paired LFP–EMG signals are correlated in any frequency contents), the depth of electrode from the dorsal surface, and a time domain analysis on lag estimation, the coherent pattern was putatively attributed to motoneuron pool activity (***Takei and Seki, 2008***). However, potent evidence for this claim was lacking such as similarities in the spatiotemporal patterns and the directionality of information transfer, concomitant with more accurate lag estimation in a particular direction. Here, we found broad-band coherent pat-

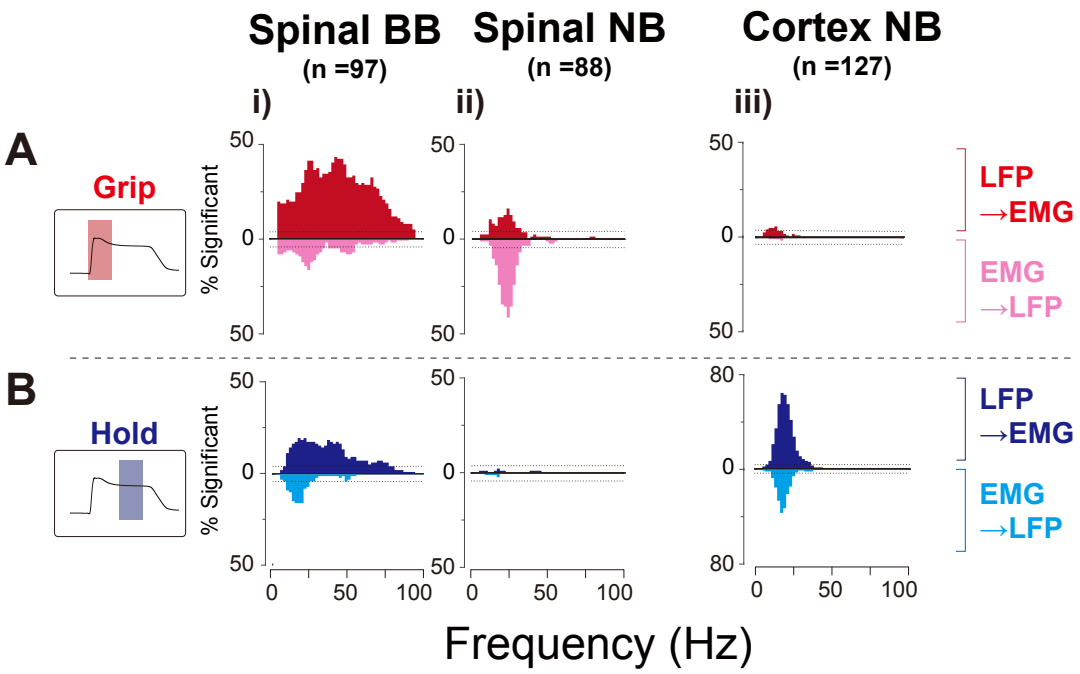

Figure 6. Pooled directed coherence distributions of significant frequency bands for efferent (LFP to EMG: red for grip, blue for hold) and afferent (EMG to LFP: magenta for grip, cyan for hold) components of directed coherence for grip **(A)** and hold **(B)** phases. Each horizontal line represents the significance level (binomial parameter estimation with $p = 0.005$). Spinal broad-band coherence predominantly consists of efferent components in both grip and hold phases, with relatively smaller effects from the afferent components in the beta band (**A**, i) and **B**, i)). Spinal NB in the grip phase comprises beta-range efferent and afferent components, with an afferent prevalence (**A**, ii)). Cortical NB comprises a bidirectional interaction through efferent and afferent components in the beta band, with an efferent prevalence (**B**, iii)).

terns closely resemble typical temporal EMG profiles (i.e., phasic-tonic activity) (Figure 1D-i, 2A-i, 2B-i, ***Takei and Seki*** (***2013a***)), and spatial distribution over the recruited muscles (Figure 3B). Directional information analyses based on MVAR further indicate that the broad-band transfer was exclusively efferent from the spinal LFPs to the muscles (Figure 6A-i, 6B-i), with a physiologically-plausible lag (c.a. 8-9 ms, Figure 7A-i, 7B-i, ***Maier et al.*** (***1998***)). Collectively, spinomuscular coherence with a broad range of frequencies represents a direct transfer of a signal between the motoneuron pool and the innervated muscles.

Beta-range coherence in the spinal cord and motor cortex emerge in distinct phases, forming separate bidirectional loops

Most of the beta-band coherence in the spinal cord were observed during the grip phase (Figure 2A-ii, 2B-ii). To the best of our knowledge, this is the first report on a neural structure showing noticeable beta-range coherence with the muscles during the dynamic phase of movement. We initially hypothesized that the coherent pattern would reflect convergence of efferent motor desynchronized discharge upstream in the descending pathway (***Baker et al., 1999***, ***2003***) and hence, would occur prior to the onset of muscle activity. However, the spinal beta coherence pattern lagged behind the motoneuron pool activity that was reflected by the broad-band coherence (Figure S2). Further, the coherence did not consist of a unidirectional information transfer, but a bidirectional interaction with dominant afferent components to LFPs from EMGs (Figure 6A-ii). These findings indicate that the spinomuscular coherence evident in the dynamic phase reflects a feedback-mediated interaction between the spinal structure and the muscles, rather than a convergent efferent command relayed from the motor cortex to the muscles. The feedback is likely induced by mechanical events associated with the contraction of a muscle (e.g., a stretch of skin and a length and tension change

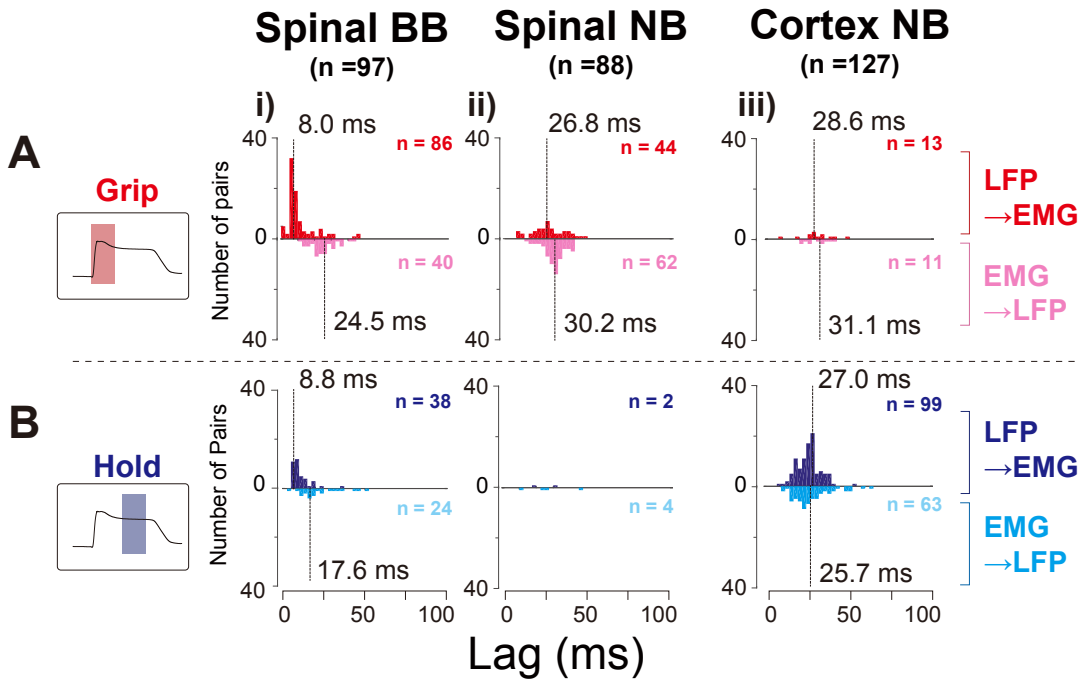

Figure 7. Distributions of phase lag of partial directed coherence for efferent and afferent components. The number of significant pairs, as determined by directed coherence analysis (Figure 6), are shown at the upper right for each distribution. Captions and arrangements of the histograms are the same as in Figure 6. The lags for efferent components for spinal BB are as short as the conduction delay from the motoneuron pool to the muscle (**A**-i) and **B**-i)). The efferent and afferent lags for cortical NB are comparable to those of the spinal NB afferent components (**A**-iii) and **B**-iii) vs. **A**-ii) and **B**-ii)). The aggregate lags for the afferent and efferent components of the spinal NB and cortical NB are approximately 50 ms, which corresponds to the whole cycle duration of beta-range oscillation.

of the contracting muscle). In effect, the latencies of the afferent components correspond by and large to that of the peak responses of spinal interneurons to a mechanical perturbation against the wrist (***Fetz et al., 2002***), suggesting that the afferent component of the coherence reflects a somatosensory feedback, including cutaneous and proprioceptive information. Such afferent components were also found in the spinal broad-band coherence (Figure 6A-i, 6B-i), suggesting that part of the somatosensory feedbacks reaches in close proximity to the motoneuron pool. Such an interaction might reflect a monosynaptic reflex arc (e.g., Ia monosynaptic reflex). Indeed, neurons in the dorsal root ganglion (DRG) defined as Ia afferent neurons exhibit a sizable magnitude of coherence through a bidirectional interaction with the innervated muscles (***Baker et al., 2006***). In addition, the sum of the medians of the phase delays for the afferent and efferent components of spinal beta coherence quantitatively matched with the cycle duration in the beta range (Figure 7A-ii).

Taken together, beta-band spinomuscular coherence emerging through a feedback loop probably arises from cutaneous and proprioceptive receptors, which may be triggered by mechanical events associated with muscle contraction. More complete understanding would be obtained if one could find spinal premotoneuronal neurons that respond to sensory stimuli are synchronized with the beta oscillation in the dynamic phase of the grip.

In contrast, corticomuscular coherence in the beta band was pronounced predominantly during the hold phase (Figure 2A-iii, 2B-iii), confirming the results extensively reported in numerous previous studies (***Conway et al., 1995***; ***Baker et al., 1997***, ***1999***; ***Salenius et al., 1997***; ***Kilner et al., 1999***; ***Kristeva et al., 2007***). However, the question regarding how the coherence emerges remains unanswered. One hypothesis states that it reflects an efferent entrainment of oscillatory cortical drive observed at the muscle (***Gerloff et al., 2006***), whereas another suggests that the coherence

arises through a reciprocal interaction of motor commands and sensory feedbacks between the cortex and the muscles (***Baker, 2007***; ***Aumann and Prut, 2015***).

The unresolved key analysis to addressing this question is the lag estimate; the lag estimates obtained in the previous studies were widely dispersed, sometimes out of the range of the beta band (i.e., less than 30 ms or more than 60 ms) (***Witham et al., 2010***, ***2011***). This is likely due to an inherent estimation error in the directed coherence measures, as they have limited ability to dissociate direct and indirect influences on the output node (***Schouten and Campfens, 2012***; ***Campfens et al., 2013***). Particularly in a nested closed loop, an effect of previous the cycle, which is delayed in a fixed time, can induce phase shifts as a function of the frequency, thereby resulting in a deviation in lag estimates. The partial directed coherence measure, which was proposed as a means of distinguishing direct influences from indirect ones (***Baccalá and Sameshima, 2001***), can provide a rather accurate estimate of lag in the closed loop (***Campfens et al., 2013***). Using the combination of directed coherence and partial directed coherence, we obtained phase lags with tighter distributions as compared with ones reported in the previous studies (Figure 7B-iii). The sum of the medians of the phase delays for corticomuscular afferent and efferent pathways quantitatively matched with the cycle duration in the beta range. These results indicate that corticomuscular coherence is the results of a reciprocal interaction between the motor cortex and muscles in the hold phase.

Thus, our results indicates that both of spinomuscular and corticomusclar coherence emerge through separate bidirectional sensorimotor feedback loops for each dynamic and static phase. It would be intriguing if these separate loops are interacting with other. Further studies are warranted to investigate such a corticospinal interaction relevant to dynamic vs. static control of the limb.

Associations of spinomuscular and corticomuscular feedback loops with mechanically-induced short- and long-latency corrective responses

Considering the sensory feedback loops that engage motor outputs through the trans-spinal and trans-cortical loops, we conceived that these loops may share routes with the short- and long-latency corrective responses to a mechanical perturbation, for the research of a feedback controller utilized for motor control (***Scott, 2012***, ***2016***). Thus, we discuss some commonalities between the feedback loops and such corrective responses.

The short latency response is the spinal-mediated, fastest (20–50 ms) response via sensory afferents that is elicited by a local cutaneous and proprioceptive interaction, concomitantly leading to homonymous or synergistic muscle contractions (***Pierrot-Deseilligny and Burke, 2005***). These features are congruent to those of the spinomuscular loop; its latency is comparable to the short latency response (Figure 7A-ii), and it conceivably emerges via cutaneous and proprioceptive feedbacks (***Baker et al., 2006***). Furthermore, it is predominantly observed in FDI and FDPr (Figure 3A, B), both of which are prime movers of the forefinger that stretch and contract during a precision grip. In addition, putative inter-muscle interactions observed through the spinomuscular coherence are largely confined to local or synergistic muscles of FDPr (extrinsic hand flexors and wrist flexors (Figure 5A).

The long-latency response is routed via the trans-cortical pathway with a latency of 50–100 ms (***Cheney and Fetz, 1984***; ***Pruszynski et al., 2011***). This response is modifiable in a task-relevant manner; the response is evoked to a stretch of task-defined, broader range of muscles and adjacent mechanoreceptors via a musculoskeletal interaction, and directed flexibly to the task-related muscles, even beyond the joints, to achieve functionally-oriented compensation (***Kurtzer et al., 2009***; ***Cole et al., 1984***; ***Pruszynski and Scott, 2012***). Likewise, corticomuscular coherence was observed in a broad range of finger muscles, including intrinsic and extrinsic hand flexor muscles (Figure 3B), with putative connections among the muscles being divergent, as reflected by muscle combinations simultaneously observed through corticomuscular coherence (Figure 5B). These hand muscles are mechanically linked through various joints and tendons, and thus their complex mechanical interactions may elicit cutaneous and proprioceptive feedbacks across the muscles, which are concomitantly routed back to various muscles. To stabilize the grip hold, it would be

necessary to respond to normal and tangential force errors by supporting the digits from various directions by co-contracting various muscles across the joints. Indeed, it has been demonstrated that the CM system, in which many cells show sustained activities during the hold period, plays a role in joint fixation by recruiting the cells with various (e.g., synergistic, fixator, and antagonistic) target muscles (***Griffin et al., 2015***; ***Lemon, 2019***).

Taken together, despite the lack of direct comparative evidence, it is worth noting the common characteristics between the separate trans-spinal and trans-cortical feedback loops, and sophisticated corrective responses to mechanical perturbation with respect to mediated pathways, latencies, and involved muscles. Further studies are required to directly explore these identities.

Comparison of neural circuitry implementation for dynamic vs. static control between saccadic and prehensile movements

The separation of engaged feedback loops in the dynamic and static phases indicates phase-specific, dedicated circuits at work in the dexterous hand control. This finding is a clearer indication of the implementation of dedicated circuits for dynamic and static control in the skeletomotor system, as compared with the moderate gradation in proportions of neuronal discharge properties between the dynamic and static phases (***Crammond and Kalaska, 1996***; ***Maier et al., 1993***; ***Griffin et al., 2015***; ***Shalit et al., 2012***; ***Takei and Seki, 2013a***). Conceptually, the separation of the circuitry for each phase appears common to the neural circuit implementation for saccadic eye movements accommodated in the brainstem (***Robinson, 1973***; ***Jürgens et al., 1981***; ***Shadmehr, 2017***).

However, there is a clear difference between the oculomotor and skeletomotor circuitry; the oculomotor circuitry rests its function on internal circuits for generating sustained activity (neural integrator), and monitoring displacement (displacement integrator) (***Robinson, 1973***; ***Jürgens et al., 1981***; ***Shadmehr, 2017***). Distinctively, in the skeletomotor system, feedbacks arising from sensory afferents seem to be used more for both dynamic and static control. In the dynamic phase, the trans-spinal feedback loop may contribute to accumulating motor commands in a recursive manner such that it works as if a “neural integrator”, whereas in the static phase, displacement monitoring and motor adjustment may be achieved through sensory afferent feedback loops via the supraspinal structure. These features never exclude putative contributions from an internally generated, feedforward command that may have eluded coherence analyses.

Nevertheless, at least in part, these different degrees of dependence on afferent information may be explained by their physical properties and interacting environments. As compared with the oculomotor system, the skeletomotor control system (developed later phylogenically) needs to control heavier, redundant multi-articulated effectors with a larger inertia under larger gravitational influences. In these conditions, the system is more susceptible to disturbance and motor noises (***Harris and Wolpert, 1998***; ***Faisal et al., 2008***). With such inherent variability of outputs arising from the effector, it would be difficult to precisely anticipate how much activity would be required to displace and sustain the limb in place. To adapt for this demand, the neural system for skeletomotor control may have shifted its dependence onto feedback control by utilizing afferent information (***Todorov, 2004***).

Conclusions

The findings of this study highlight that two separate feedback controllers, as reflected by trans-spinal and trans-cortical feedback loops via phase-specific coherence patterns, may also be utilized for goal directed, voluntary dynamic and static control of grip. This insight potentially provides a broader framework for understanding in voluntary dynamic and static control of our body from a feedback control perspective. In addition, the insight is particularly helpful to consider functional roles of neural coherence, as it is still debated in recent studies what corticomuscular coherence specifically represents; a motor command for holding the displacement (***Baker et al., 1999***), active sensing such as the rodent whisker system (***Baker, 2007***; ***MacKay, 1997***), recalibration signals (***Baker,***

2007) or neural gain mechanisms that facilitate sensorimotor interactions (***Schoffelen et al., 2005***; ***Womelsdorf et al., 2007***). Our results lend supports to functions arising from a neural–muscle–neural loops, probably related to a feedback controller, providing a direction for designing a more desirable task framework to elucidate the functional roles of the sensorimotor loop for dynamic and static motor control.

Methods and Materials

Dataset

The datasets used in the present study were obtained from four male macaque monkeys consisting of three *Macaca fuscata* (monkey U: 8.5 kg, monkey A: 6.8 kg, monkey S: 9.0 kg) and one *Macaca mulatta* (monkey E: 5.6 kg). Spinal cord datasets were obtained from monkeys U, A, and E; cortical datasets were obtained from monkeys E and S, respectively. All experimental procedures described below were approved by the Animal Research Committee at the National Institute for Physiological Sciences, and National Center of Neurology and Psychiatry, Japan.

Behavioral task

Each monkey was trained to squeeze a pair of spring-loaded levers with its left index finger and thumb (precision grip task; Figure 1A, B) (***Takei and Seki, 2008***, ***2013a***). The monkey was instructed to track defined targets in a step-tracking manner by squeezing the spring-loaded levers, the positions of which were displayed on a computer screen as cursors. Each trial comprised a rest period (1.0–2.0 s), lever grip, lever hold (1.0–2.0 s), and lever release (Figure 1B). On successful completion of the trial, the monkey was rewarded with a drop of apple puree. The force required to reach the target positions was adjusted independently for the index finger and thumb of each individual monkey.

Surgical procedures

After the monkeys had learned the required task for a sufficient time period, we performed surgeries to implant head restraints, EMG wires, and recording chambers under isoflurane or sevoflurane anesthesia and aseptic conditions. For EMG recordings from forelimb muscles, we performed a series of surgeries to subcutaneously implant pairs of stainless steel wires (AS 631, Cooner Wire, CA, USA) acutely or chronically. Specific muscle sets (ranging from intrinsic hand to elbow muscles) for each animal are listed in Table S1. For spinal recordings, we implanted a recording chamber on the cervical vertebra (C4–C7) of monkeys U, A, E and S where a unilateral laminectomy was made on the ipsilateral side of the employed hand and arm. After completion of the spinal recordings, we performed a surgery on monkeys E and S to implant a recording chamber (a circular cylinder with a 50-mm diameter) over the skull where a craniotomy was made covering a cortical area, including the hand representation of pre- and post central gyri on the contralateral side of the employed hand and arm.

Neurophysiological recordings

While the monkey performed the precision grip task, we recorded the local field potentials (LFPs) from the spinal C5–T1 segments, or from the hand area of the motor cortex through the chamber attached either on the spinal vertebrae or on the cranium by inserting a tungsten or Elgiloy alloy microelectrode (impedance: 1 – 2 MΩ at 1 kHz) with a hydraulic microdrive (MO-951, Narishige Scientific Instrument, Japan). The recording sites were explored with aid of positions of vertebral segments for the spinal recordings, and the geometric information adjacent to the central sulcus and electrical miscrostimulation for the cortical recordings. The LFP signals were referenced to a silver ball electrode placed on a surface of dura mater of spinal cord or cerebral cortex, thereafter amplified (1000 times), band-pass filtered between 0.1 Hz and 10 kHz using a differential amplifier (Model 180, A-M Systems, WA, USA), and digitized at 20 kHz. The EMGs were amplified (3000–25000

times) and filtered (between 5 Hz and 3 kHz) using a multichannel differential amplifier (SS-6110, Nihon Kohden, Japan) and digitized at 5 kHz. Signals from the potentiometers and strain gauges attached to levers, and from the capacitive touch sensors were digitized at 1 kHz.

Data analysis

All subsequent analyses were carried out off-line using custom-written scripts in a MALTAB environment (Mathworks, Natick, MA, USA). Only LFP–EMG pairs that had > 99 trials of the data were averaged for analysis, and LFPs from the intraspinal or intracortical sites < 150 μm apart were pooled to avoid redundancies resulting from propagation of the potential.

Grip onset was defined as the time at which the rate of change in the aggregate grip force (sum of forces exerted by the index finger and thumb) exceeded 2 N/s. Release onset was, likewise, determined as the time at which the rate of change in the grip force reduced below -2 N/s.

LFPs were band-pass filtered (4th-order Butterworth filter between 3 and 100Hz) and down-sampled to a 250 Hz sampling rate. EMGs were high-pass filtered at 30 Hz (4th-order Butterworth filter), rectified, and down-sampled to 250 Hz.

Electrical cross talk among EMGs

To exclude spurious coherence arising from electrical cross-talk among EMGs, we quantified the degree of electrical cross talk among EMGs recorded simultaneously using a method developed by ***Kilner et al.*** (***2002***). Original EMGs were down-sampled to 1 kHz and differentiated three times without being rectified. The preprocessed signals were then subjected to cross correlation analysis given as:

$$r(\tau) = \frac{\frac{1}{t_{max}} \sum_{i=0}^{t_{max}} f_1(t) f_2(t-\tau) - \overline{f}_1 \overline{f}_2}{\sigma_1 \sigma_2} \tag{1}$$

where f_1 and f_2 are two differentiated EMG signals, $\overline{f}_1$ and $\overline{f}_2$ are their mean values, and σ_1 and σ_2 are their standard deviations. r was calculated with 25-ms lags and a maximum modulus of r, $|r|_{max}$, was used as an index of the extent of cross-talk. In each experimental day, $|r|_{max}$ was calculated between EMG signals of every simultaneously recorded muscle pair for a 1-min epoch. We set a significant cross talk threshold to 0.25 for each muscle pair, and in cases where it exceeded the threshold, we randomly excluded either one of the pair from the data pool. Also, to eliminate any influence from the power line, we excluded the frequency band between ± 5 Hz with regard to 50 (monkeys U, A, and E) or 60 (monkey S) Hz, and concatenated the neighboring frequencies.

Time Frequency Representation: Wavelet coherence

To analyse the time series containing nonstationary power at different frequencies, we employed a coherence analysis between wavelet-transformed signals. LFP and EMG signals spanning either an onset of grip or an onset of hold release (from 1 s before and 0.5 s after each onset) were transformed using complex gabor wavelets (σ = 128 ms) (Figure 1D, top traces for LFPs and middle traces for EMGs). We thereafter calculated the coherence between the transformed LFPs and EMGs (Figure 1D, bottom traces), as per the equation below:

$$Coh(t,f) = \frac{|\frac{1}{N} \sum_{j=1}^{N} X_j(t,f) Y_j(t,f)|^2}{P_X(t,f) P_Y(t,f)} \tag{2}$$

where X and Y are time frequency representations and P_X, P_Y are power spectra of LFP and EMG signals calculated using the wavelet transformation.

Coherence in a fixed time window: standard coherence

To compare the coherence measures in the grip and hold phases, we took time windows from 0 to 512 ms after grip onset for the grip phase and from 768 to 256 ms prior to the release onset for the hold phase for analysis. Thereafter, 128-point time series were divided into non-overlapping

segments for Fast Fourier Transform (FFT). This allowed investigation of spectral measurements with a frequency resolution of 1.95 Hz. We then calculated one-sided power spectra for the 128-point time series of LFP and EMG signals. Denoting the Fourier transform of the *i*th section of LFPs and EMGs as $F_{1,j}(f)$ and $F_{2,i}(f)$, respectively, the power spectrum of each signal (*j*=1,2) was calculated as:

$$P_j(f) = \frac{2}{256^2 L} \sum_{i=1}^{L} F_{j,i}(f) F_{j,i}^*(f) \tag{3}$$

where *L* is the number of data segments available and * denotes the complex conjugate (***Witham et al., 2007***). Using this normalization, $P(f)$ has units of μV^2.The calculation of coherence between an LFP–EMG pair is as follows:

$$Coh(f) = \frac{|\sum_{i=1}^{L} F_{1,i}^*(f) F_{2,i}(f)|^2}{\sum_{i=1}^{L} F_{1,i}^*(f) F_{1,i}(f) \sum_{i=1}^{L} F_{2,i}^*(f) F_{2,i}(f)} \tag{4}$$

A significance threshold level *S* was calculated according to ***Rosenberg et al.*** (***1989***) as

$$S = 1 - \alpha^{\frac{1}{L-1}} \tag{5}$$

where α is the significance level. Because we were more interested in detecting coherence bands, spurious point-wise significance had to be excluded. Thus, we put a more stringent level for the probability, i.e., α = 0.005, corresponding to a threshold coherence value S of 0.0409.

Classification of coherence types

To classify qualitatively different time-frequency patterns of LFP–EMG coherence 1D, we quantitatively characterize those patterns based on two features of coherence measures; an integral of contours of wavelet coherence (Figure S1A-i) and a frequency width of standard coherence (Figure S1A-ii). The integral of contour was quantified as a volume that exceeded a significant level in a time window from 0 to 1 s with regard to the grip onset for grip, or a time window from -1 to 0 s from the onset of hold release, thereby reflecting coherence strength, how wide its significant frequency band distributes, and how long the coherency extends over time. To dissociate two types of spinomuscular coherence, We then applied the Expectation–Maximization (E–M) algorithm to the distribution of integral of contours, under a Gaussian mixture model (GMM) assumption (***Bishop, 2006***). Points assigned as narrow-band in the contour integral dimension were examined for outliers in the frequency width dimension (Smirnov-Grubbs test, $p < 0.05$). Three points were determined as outliers and exceeded 25 Hz in frequency width; a criterion used for classification in the previous study (***Takei and Seki, 2008***). We therefore assigned those points to the broad-band category.

Comparison of frequency distributions between spinal narrow-band and cortical narrow-band coherence

For comparison of frequency distributions between the spinal narrow-band and cortical narrow-band coherence patterns, the normalized (*Z*-transformed) differences between the two patterns of coherence were tested using the nonparametric Monte Carlo method (***Maris et al., 2007***). The *Z*-transformation was undertaken as:

$$Z = \frac{\left(atanh(|C_1(f)|) - \frac{1}{DF_1 - 2}\right) - \left(atanh(|C_2(f)|) - \frac{1}{DF_2 - 2}\right)}{\sqrt{\left(\frac{1}{DF_1 - 2}\right) + \left(\frac{1}{DF_2 - 2}\right)}} \tag{6}$$

where $|C_1(f)|$ and $|C_2(f)|$ stand for each coherence, and DF_1 and DF_2 for the degrees of freedom (2 x (pairs) x (frequency bin)). Under the null hypothesis the two coherence frequency distributions are equal, the underlying datasets ((88 pairs against 127 pairs) x (64 frequency bins)) for two coherence patterns were randomly permuted, averaged, and calculated into the *Z*-scores above.

The procedure was iterated 10000 times to obtain an empirical distribution, from which 97.5th and 2.5th percentiles were assigned for upper and lower limits to determine a significance (Figure 4A-ii).

Spectral analysis on the Multivariate Autoregressive (MVAR) model

Given the significant coherence found between LFPs and EMGs in the grip or hold phase, we further sought to examine whether the coherence reflects putatively causal interactions with a particular direction. Analyses of the causal interaction in the network can involve estimating the extent to which one signal influences another, and assessing whether the lags between them based on the measure are (physiologically) plausible.

For this purpose, we performed spectral analysis on the multivariate autoregressive (MVAR) model (***Kamiński and Blinowska, 1991***), that was estimated from the LFP and EMG time series in the same time window as used for standard coherence; 512 ms (128 points). The segmented signals were fitted to an MVAR model of two time series (ARfit package (***Schneider and Neumaier, 2001***)) as described by the equation below:

$$\begin{bmatrix} y_1(n) \\ y_2(n) \end{bmatrix} = \sum_{k=1}^{p} A_k \begin{bmatrix} y_1(n-k) \\ y_2(n-k) \end{bmatrix} + \begin{bmatrix} \epsilon_1(n) \\ \epsilon_2(n) \end{bmatrix} \tag{7}$$

where $y_1(n)$ and $y_2(n)$ are the two time series. The off-diagonal components of the 2-by-2 matrix A_k predict the current sample (n) of y_1 and y_2 from the kth past sample of y_1 and y_2. The model order p defines the maximum lag used to quantify such interactions. When the prediction error ϵ is minimized in the fitting of the coefficients of A_k, if the variance of ϵ_1 is reduced by including the y_2 terms in the first equation in (7), then based on Granger causality, one can state that y_2 causes y_1, and vice versa.

The spectral representation of the MVAR process is derived considering the Fourier transformation of the equation above (7):

$$A(f) \begin{bmatrix} y_1(f) \\ y_2(f) \end{bmatrix} = \begin{bmatrix} \epsilon_1(f) \\ \epsilon_2(f) \end{bmatrix} \tag{8}$$

where $A(f)$ is 2-by-2 coefficient matrix calculated as:

$$A(f) = \sum_{k=1}^{p} A_k \mathrm{e}^{-i2\pi f k T} \tag{9}$$

where i is an imaginary unit, and T is the sampling interval. The equation (8) is rewritten as:

$$\begin{bmatrix} y_1(f) \\ y_2(f) \end{bmatrix} = H(f) \begin{bmatrix} \epsilon_1(f) \\ \epsilon_2(f) \end{bmatrix} \tag{10}$$

where $H(f)$ is 2-by-2 *transfer function matrix* calculated with $A(f)$:

$$H(f) = [I - A(f)]^{-1} = \bar{A}(f) \tag{11}$$

where I is the identity matrix.

Considering the trade-off between sufficient spectral resolution and overparameterization, we determined the model order as a value of 15 (60 ms for our 250 Hz sampling rate), as a comparable value of 10 (50 ms for 200 Hz sampling rate) was used in the previous study that focused on an MVAR model of sensorimotor cortical networks underlying the beta oscillation (***Brovelli et al., 2004***).

Directed coherence and partial directed coherence

We then derived two measures based on the transfer function matrix $H(f)$ or the coefficient matrix $A(f)$ in the MVAR spectral model, one called directed coherence (***Baker et al., 2006***), while the other called partial directed coherence (***Baccalá and Sameshima, 2001***).

Directed coherence ($\gamma_{ij}(f)$) is calculated as:

$$\gamma_{i\leftarrow j}(f) = |H_{ij}(f)|^2 \frac{S_{jj}(f)}{S_{ii}(f)} \tag{12}$$

where $S_{kk}(f)$ is the power spectral density of the signal k, calculated based on the AR model as:

$$S(f) = H(f)V H(f)^H \tag{13}$$

where V is the covariance matrix of the error term $\epsilon(f)$ and the superscript H denotes the Hermitian conjugate.

Partial directed coherence ($\pi_{ij}(f)$) is calculated as follows:

$$\pi_{i\leftarrow j}(f) = \frac{\frac{1}{\delta_i^2}|\bar{A}_{ij}(f)|^2}{\sum_{m=1}^{M}\frac{1}{\delta_m^2}|\bar{A}(f)_{mj}|^2} \tag{14}$$

where δ_k represents a variance of u_k.

Partial directed coherence ($\pi_{ij}(f)$), reflecting the off-diagonal elements of $A(f)$, is nonzero if and only if direct causality from y_j to y_i exists, whereas directed coherence ($\gamma_{ij}(f)$), based on $H(f)$ that contains a sum of terms related to every transfer paths, is nonzero whenever any path connecting y_j to y_i is significant, reflecting both direct and indirect causality between y_j and y_i. The two measures also differ in normalization; $\gamma_{ij}(f)$ is normalized with respect to the structure that receives the signal, whereas $\pi_{ij}(f)$ is normalized with respect to the structure that sends the signal.

As such, directed coherence provides a total causal influence as the amount of signal power transferred from one process to another but can not distinguish direct causal effects from indirect ones. Conversely, partial directed coherence clearly measures the underlying interaction structure as it provides a one-to-one representation of direct causality, but is hardly useful as a quantitative measure because its magnitude quantifies the information outflow, which does not provide precisely how much information reaches downstream.

Documented directed coherence measures applied to corticomuscular interactions (***Baker et al., 2006***; ***Tsujimoto et al., 2009***; ***Witham et al., 2010***, ***2011***) have limited accuracy in estimating the phase-lag relationship, due to their inability to distinguish the direct and indirect causal effects. This is probably because the sensorimotor corticomuscular interaction comprises closed loops, including a bidirectional interaction between the motor cortex and the muscles (***Schouten and Campfens, 2012***; ***Campfens et al., 2013***). In a nested loop, an oscillation in the past cycle would be recurrently summed, thereby leading to a phase shift owing to the synthesis of oscillations separated with a fixed time lag of the loop cycle. The degree of phase shift is variable for different frequency bands; when a lag in the time domain is converted to a phase in the frequency domain, the phase is increased as a function of the frequency band. Hence, an estimate of a lag based on a phase-lag plot tends to be shorter than actual transmission, as demonstrated by ***Campfens et al.*** (***2013***). The authors further showed in the simulation that partial directed coherence provided the most accurate estimate of the lag that any other directed coherence measures never attained. This is a clear indication that partial directed coherence reflects a direct causal relationship between the two variables as theoretically explained above.

Considering the complementary properties of directed coherence and partial directed coherence measures, we decided to employ directed coherence to determine a causal influence between the cortex and muscles, and partial directed coherence to measure the phase-lag relationship for the causally defined interaction by directed coherence. By combining these two measures, we can reliably determine causal influences between the cortex and the muscles, and can also estimate the lag accurately in the presence of open or closed loops interposed in between.

Baker et al. (***2006***) showed that the significance limit of directed coherence was comparable with that for standard coherence as stated in equation (5). Based on this assumption, we set α level as the same value for the coherence analysis as for directed coherence (p = 0.005). For

statistical tests on combined coherence across multiple recorded pairs (pooled coherence), we chose a nonparametric method according to ***Baker et al.*** (***2003***) wherein we simply counted the percentage of bins at a particular frequency that exceeded the significance limit in the individual coherence spectra. The percentage was calculated by dividing the significant number by the total number of pairs at a given frequency, and the significance limit was determined using binomial parameter estimation (p = 0.005) with the total number of pairs.

The phase of partial directed coherence for the significant bins determined by directed coherence was calculated as follows:

$$\theta(f) = arg\left(\sum_{i=1}^{L} X_i^*(f)Y_i(f)\right) \tag{15}$$

where L is the number of the data sections, X and Y denote each time series, and $*$ denote complex conjugate. The 95% confidence limits on the phase estimates, $(\theta \pm \Delta\theta)$ were determined according to ***Rosenberg et al.*** (***1989***):

$$\Delta\theta(f) = 1.96\sqrt{\frac{1}{2L}\left(\frac{1}{Coherence(f)} - 1\right)} \tag{16}$$

To determine if there is a fixed time delay between the two time series, we fitted a regression line to the phase-frequency relationship, as two correlated signals with a fixed time delay in the time domain give a linear function of frequency in the spectral domain. If the slope is significantly different from zero $p < 0.05$, t-test on the regression coefficient), the constant delay (τ ms) was estimated from the line's slope as follows:

$$\tau = -\frac{1000}{2\pi}A \tag{17}$$

where A is the line's slope (rad/Hz). A negative slope (positive delay) indicates that LFP leads EMG with a constant delay and vice versa.

Acknowledgments

The authors would like thank C. Sasaki, N. Takahashi and K. Isa for technical assistance. This work was supported by JSPS Grants-in-Aid (KAKENHI) Grant Numbers; 18020030, 18047027, 20020029, 20033025, 23300143, 26120003, 26250013 (to K.S.), 06J02928, 21700437, 23700482 (to T.T.), 10J05147, and 18K10984 (to T.O.). K.S. was funded by JST Precursory Research for Embryonic Science and Technology Program.

References

Aumann TD, Prut Y. Do sensorimotor β-oscillations maintain muscle synergy representations in primary motor cortex? Trends in Neurosciences. 2015; 38(2):77–85.

Baccalá LA, Sameshima K. Partial directed coherence: a new concept in neural structure determination. Biological Cybernetics. 2001; 84(6):463–474.

Baker SN, Kilner JM, Pinches EM, Lemon RN. The role of synchrony and oscillations in the motor output. Experimental Brain Research. 1999; 128(1-2):109–117.

Baker SN, Olivier E, Lemon RN. Coherent oscillations in monkey motor cortex and hand muscle EMG show task-dependent modulation. The Journal of Physiology. 1997; 501(1):225–241.

Baker SN. Oscillatory interactions between sensorimotor cortex and the periphery. Current Opinion in Neurobiology. 2007; 17(6):649–655.

Baker SN, Chiu M, Fetz EE. Afferent encoding of central oscillations in the monkey arm. Journal of Neurophysiology. 2006; 95(6):3904–3910.

Baker SN, Pinches EM, Lemon RN. Synchronization in Monkey Motor Cortex During a Precision Grip Task. II. Effect of Oscillatory Activity on Corticospinal Output. Journal of Neurophysiology. 2003; 89(4):1941–1953.

Bishop CM. Pattern Recognition and Machine Learning. Springer Verlag; 2006.

Brovelli A, Ding MZ, Ledberg A, Chen YH, Nakamura R, Bressler SL. Beta oscillations in a large-scale sensorimotor cortical network: Directional influences revealed by Granger causality. Proceedings of the National Academy of Sciences. 2004; 101(26):9849–9854.

Campfens SF, van der Kooij H, Schouten AC. Face to phase: pitfalls in time delay estimation from coherency phase. Journal of Computational Neuroscience. 2013; 37(1):1–8.

Cheney PD, Fetz EE. Corticomotoneuronal cells contribute to long-latency stretch reflexes in the rhesus monkey. The Journal of Physiology. 1984; 349:249–272.

Cole KJ, Gracco VL, Abbs JH. Autogenic and nonautogenic sensorimotor actions in the control of multiarticulate hand movements. Experimental Brain Research. 1984; 56(3):582–585.

Conway BA, Halliday DM, Farmer SF, Shahani U, Maas P, Weir AI, Rosenberg JR. Synchronization between motor cortex and spinal motoneuronal pool during the performance of a maintained motor task in man. The Journal of Physiology. 1995; 489(3):917–924.

Crammond DJ, Kalaska JF. Differential relation of discharge in primary motor cortex and premotor cortex to movements versus actively maintained postures during a reaching task. Experimental Brain Research. 1996; 108(1):45–61.

Divekar NV, John LR. Neurophysiological, behavioural and perceptual differences between wrist flexion and extension related to sensorimotor monitoring as shown by corticomuscular coherence. Clinical neurophysiology. 2013; 124(1):136–147.

Faisal AA, Selen LPJ, Wolpert DM. Noise in the nervous system. Nature Reviews Neuroscience. 2008; 9(4):292–303.

Fetz EE, Perlmutter SI, Prut Y, Seki K, Votaw S. Roles of primate spinal interneurons in preparation and execution of voluntary hand movement. Brain Research Reviews. 2002; 40(1-3):53–65.

Gerloff C, Braun C, Staudt M, Hegner YL, Dichgans J, Krägeloh-Mann I. Coherent corticomuscular oscillations originate from primary motor cortex: Evidence from patients with early brain lesions. Human Brain Mapping. 2006; 27(10):789–798.

606 **Griffin DM**, Hoffman DS, Strick PL. Corticomotoneuronal cells are "functionally tuned". Science. 2015;
607 350(6261):667–670.

608 **Gross J**, Tass PA, Salenius S, Hari R, Freund HJ, Schnitzler A. Cortico-muscular synchronization during isometric
609 muscle contraction in humans as revealed by magnetoencephalography. The Journal of Physiology. 2000;
610 527(3):623–631.

611 **Harris CM**, Wolpert DM. Signal-dependent noise determines motor planning. Nature. 1998; 394(6695):780–784.

612 **Jürgens R**, Becker W, Kornhuber HH. Natural and drug-induced variations of velocity and duration of human
613 saccadic eye movements: evidence for a control of the neural pulse generator by local feedback. Biological
614 Cybernetics. 1981; 39(2):87–96.

615 **Kamiński MJ**, Blinowska KJ. A new method of the description of the information flow in the brain structures.
616 Biological Cybernetics. 1991; 65(3):203–210.

617 **Kilner JM**, Baker SN, Lemon RN. A novel algorithm to remove electrical cross-talk between surface EMG
618 recordings and its application to the measurement of short-term synchronisation in humans. The Journal of
619 Physiology. 2002; 538(3):919–930.

620 **Kilner JM**, Baker SN, Salenius S, Jousmäki V, Hari R, Lemon RN. Task-dependent modulation of 15-30 Hz
621 coherence between rectified EMGs from human hand and forearm muscles. The Journal of Physiology. 1999;
622 516(2):559–570.

623 **Kristeva R**, Patino L, Omlor W. Beta-range cortical motor spectral power and corticomuscular coherence as
624 a mechanism for effective corticospinal interaction during steady-state motor output. NeuroImage. 2007;
625 36(3):785–792.

626 **Kurtzer I**, Pruszynski JA, Scott SH. Long-Latency Responses During Reaching Account for the Mechanical
627 Interaction Between the Shoulder and Elbow Joints. Journal of Neurophysiology. 2009; 102(5):3004–3015.

628 **Lemon R**. Recent advances in our understanding of the primate corticospinal system. F1000Research. 2019;
629 8:274–8.

630 **MacKay WA**. Synchronized neuronal oscillations and their role in motor processes. Trends in Cognitive Sciences.
631 1997; 1(5):176–183.

632 **Maier MA**, Bennett KM, Hepp-Reymond MC, Lemon RN. Contribution of the monkey corticomotoneuronal
633 system to the control of force in precision grip. Journal of Neurophysiology. 1993; 69(3):772–785.

634 **Maier MA**, Perlmutter SI, Fetz EE. Response Patterns and Force Relations of Monkey Spinal Interneurons During
635 Active Wrist Movement. Journal of Neurophysiology. 1998; 80(5):2495–2513.

636 **Maris E**, Schoffelen JM, Fries P. Nonparametric statistical testing of coherence differences. Journal of Neuro-
637 science Methods. 2007; 163(1):161–175.

638 **Pesaran B**, Vinck M, Einevoll GT, Sirota A, Fries P, Siegel M, Truccolo W, Schroeder CE, Srinivasan R. Investigating
639 large-scale brain dynamics using field potential recordings: analysis and interpretation. Nature Neuroscience.
640 2018; 21(7):1–17.

641 **Pierrot-Deseilligny E**, Burke D. The Circuitry of the Human Spinal Cord. Its Role in Motor Control and Movement
642 Disorders, Cambridge University Press; 2005.

643 **Pruszynski JA**, Kurtzer I, Nashed JY, Omrani M, Brouwer B, Scott SH. Primary motor cortex underlies multi-joint
644 integration for fast feedback control. Nature. 2011; 478(7369):387–390.

645 **Pruszynski JA**, Scott SH. Optimal feedback control and the long-latency stretch response. Experimental Brain
646 Research. 2012; 218(3):341–359.

647 **Riddle CN**, Baker SN. Convergence of Pyramidal and Medial Brain Stem Descending Pathways Onto Macaque
648 Cervical Spinal Interneurons. Journal of neurophysiology. 2010; 103(5):2821–2832.

649 **Robinson DA**. Models of the saccadic eye movement control system. Kybernetik. 1973; 14(2):71–83.

650 **Rosenberg JR**, Amjad AM, Breeze P, Brillinger DR, Halliday DM. The Fourier approach to the identification of
651 functional coupling between neuronal spike trains. Progress in Biophysics and Molecular Biology. 1989;
652 53(1):1–31.

Salenius S, Portin K, Kajola M, Salmelin R, Hari R. Cortical control of human motoneuron firing during isometric contraction. Journal of Neurophysiology. 1997; 77(6):3401–3405.

Schneider T, Neumaier A. Algorithm 808: ARfit—a matlab package for the estimation of parameters and eigenmodes of multivariate autoregressive models. ACM Transactions on Mathematical Software. 2001; 27(1):58–65.

Schoffelen JM, Oostenveld R, Fries P. Neuronal coherence as a mechanism of effective corticospinal interaction. Science. 2005; 308(5718):111–113.

Schouten AC, Campfens SF. Directional coherence disentangles causality within the sensorimotor loop, but cannot open the loop. The Journal of Physiology. 2012; 590(10):2529–2530.

Scott SH. The computational and neural basis of voluntary motor control and planning. Trends in cognitive sciences. 2012; 16(11):541–549.

Scott SH. A Functional Taxonomy of Bottom-Up Sensory Feedback Processing for Motor Actions. Trends in Neurosciences. 2016; 39(8):512–526.

Shadmehr R. Distinct neural circuits for control of movement vs. holding still. Journal of Neurophysiology. 2017; 117(4):1431–1460.

Shalit U, Zinger N, Joshua M, Prut Y. Descending Systems Translate Transient Cortical Commands into a Sustained Muscle Activation Signal. Cerebral Cortex. 2012; 22(8):1904–1914.

Takei T, Seki K. Spinomuscular Coherence in Monkeys Performing a Precision Grip Task. Journal of Neurophysiology. 2008; 99(4):2012–2020.

Takei T, Seki K. Spinal Premotor Interneurons Mediate Dynamic and Static Motor Commands for Precision Grip in Monkeys. Journal of Neuroscience. 2013; 33(20):8850–8860.

Takei T, Seki K. Synaptic and functional linkages between spinal premotor interneurons and hand-muscle activity during precision grip. Frontiers in Computational Neuroscience. 2013; 7:40.

Todorov E. Optimality principles in sensorimotor control. Nature Neuroscience. 2004; 7(9):907–915.

Tsujimoto T, Mima T, Shimazu H, Isomura Y. Directional organization of sensorimotor oscillatory activity related to the electromyogram in the monkey. Clinical Neurophysiology. 2009; 120(6):1168–1173.

Witham CL, Riddle CN, Baker MR, Baker SN. Contributions of descending and ascending pathways to corticomuscular coherence in humans. The Journal of Physiology. 2011; 589(15):3789–3800.

Witham CL, Wang M, Baker SN. Cells in somatosensory areas show synchrony with beta oscillations in monkey motor cortex. European Journal of Neuroscience. 2007; 26(9):2677–2686.

Witham CL, Wang M, Baker SN. Corticomuscular coherence between motor cortex, somatosensory areas and forearm muscles in the monkey. Frontiers in Systems Neuroscience. 2010; 4.

Womelsdorf T, Schoffelen JM, Oostenveld R, Singer W, Desimone R, Engel AK, Fries P. Modulation of Neuronal Interactions Through Neuronal Synchronization. Science. 2007; 316(5831):1609–1612.

687 # Supplemental Information

Table S1. Recorded muscles for each animal

Muscle	monkey U	monkey A	monkey E	monkey S
Adductor Pollicis (ADP)		x	x	x
First Dorsal Interosseous (FDI)	x	x	x	x
Second Dorsal Interosseous (2DI)			x	x
Third Dorsal Interosseous (3DI)			x	x
Fourth Dorsal Interosseous (4DI)			x	x
Abductor Pollicis Brevis (AbPB)		x	x	x
Abductor Digiti Minimi (AbDM)	x	x	x	x
Flexor Digitorum Superficialis (FDS)		x	x	x
Flexor Digitorum Profundus, radial part (FDPr)		x	x	x
Flexor Digitorum Profundus, ulnar part (FDPu)		x	x	x
Palmaris Longus (PL)		x	x	x
Flexor Carpi Radialis (FCR)		x	x	x
Flexor Carpi Ulnaris (FCU)		x	x	x
Abductor Pollicis Longus (AbPL)			x	x
Extensor Carpi Radialis (ECR)		x	x	x
Extensor Carpi Ulnaris (ECU)		x	x	x
Extensor Digitorum Communis (EDC)		x	x	x
Extensor Digitorum-2,3 (ED23)		x	x	x
Extensor Digitorum-4,5 (ED45)		x		
Brachioradialis (BRD)		x	x	x
Biceps Brachii (Biceps)		x	x	x
Triceps Brachii (Triceps)			x	

Table S2. Recorded and analyzed LFP and EMG pairs in studied structures for each animal

Structure			Spinal cord		Motor cortex	
Monkey	U	A	E	S	E	S
LFP recordings	4	7	72	1	71	26
EMG recordings	2	19	20	21	20	21
LFP-EMG pairs	8	133	1440	21	1420	546
EMG cross-talk	0	73	240	12	320	111
Analyzed pairs	8	60	1200	9	1100	435

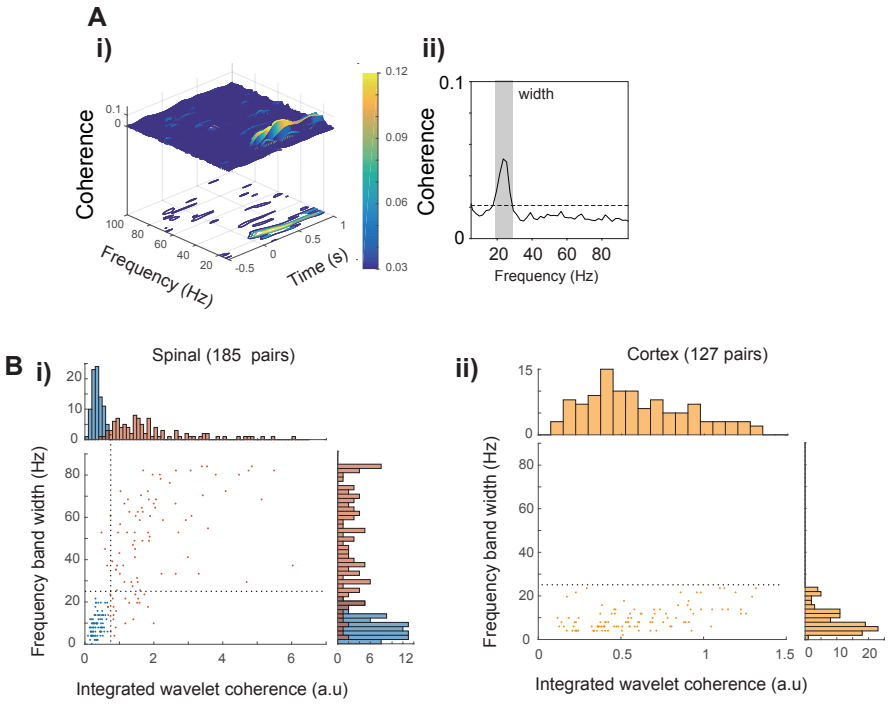

Figure S1. Group classification of coherence patterns. **A.** i) Integrated contour in wavelet coherence and ii) the frequency width in standard coherence for classification. The integrated contour was calculated as a sum of the area above the significance level from the wavelet coherence, whereas the frequency width was taken as consecutive coherence above the significance level at its highest peak (shaded area). **B.** The integrated contours (x-axis) for Spinomuscular coherence exhibited two unimodal distributions, delineating spinomuscular narrow-band and broad-band coherence, whereas corticomuscular coherence was distributed unimodally in narrow band. Using frequency band width (y-axis) some outliers (> 25Hz in frequency band width in the upper-left quadrant) in narrow-band coherence were corrected to broad band coherence.

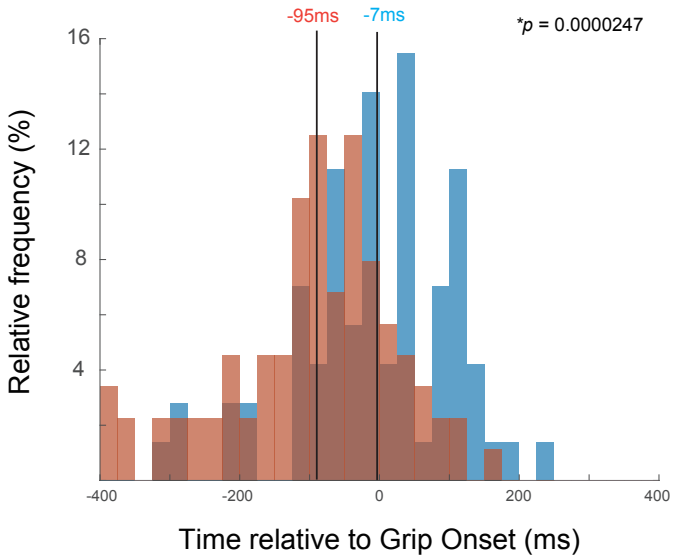

Figure S2. Comparison of latencies for spinal broad-band (BB) and narrow-band (NB) coherence with respect to grip onset. The median latency for BB (red bars: -95 ms) was significantly earlier than that for NB (blue bars: -7 ms). The *p*-value was calculated using *t*-test with unequal variance.